Optimization-based feedforward control of the strip thickness profile in hot strip rolling

authored by **K. Prinz, A. Steinboeck, and A. Kugi**

and published in *Journal of Process Control*.

Optimization-based feedforward control of the strip thickness profile in hot strip rolling

K. Prinz[a,*], A. Steinboeck[b,], A. Kugi[a]

[a]Christian Doppler Laboratory for Model-Based Process Control in the Steel Industry, Automation and Control Institute (ACIN), TU Wien, Vienna, Austria

[b]Automation and Control Institute (ACIN), TU Wien, Vienna, Austria

Abstract

A new feedforward control approach for the thickness profile of the strip in a tandem hot rolling mill is developed. In industry, the automatic gauge control (AGC) concept is widely used for thickness control. The AGC has the disadvantage that it does not consider known disturbances from upstream entities. This is why a number of disturbance feedforward control concepts have been proposed in the literature. These feedforward control strategies typically rely on linearized models and only provide symmetric control inputs for the mean thickness to the hydraulic adjustment system. In this work, an optimization-based feedforward controller for the lateral thickness profile is proposed that fully exploits all degrees of freedom available, i. e., the hydraulic cylinder positions and the bending forces at the drive side and at the operator side of the mill stand. Moreover, it is shown that by linearizing the mill stand model while keeping the nonlinearities from the roll gap model leads to a numerically efficient optimization problem, which is a good compromise between accuracy and computational efficiency. The feedforward controllers are further combined with the AGC in the feedback path in a two-degree-of-freedom controller structure to account for model-plant mismatch. Simulation results for a validated mathematical model and first experimental results from an industrial pilot installation show a significant benefit compared to the existing AGC without feedforward control.

Keywords: Hot strip rolling, Metals industry, Thickness control, Shape and profile control, Model-based optimization, Feedforward control

Nomenclature

Abbreviations

AGC	Automatic gauge control
BR	Backup roll
CVC	Continuous variable crown
DS	Drive side
FF	Feedforward control
HGC	Hydraulic gap control
MIMO	Multiple input, multiple output
OS	Operator side
SISO	Single input, single output
TCW	Thermal and wear crown
WR	Work roll
WRB	Work roll bending
WRS	Work roll shifting

Variables

x, y, z	Cartesian coordinates
$\tilde{b}$	Parameter used in cost function
b_{br}	Distance between hydraulic cylinders
b_c	Face length of backup roll
b_R	Material width
b_{wrb}	Distance between hydraulic WRB cylinders
c_m	Mill modulus
c_i	Crown of the roll
e	Thickness error defined in cost function
F_B	Force applied to the BR bearing
F_f	Frictional force
F_R	Roll force
F_{bal}	Balancing force
F_h	Force of the hydraulic main cylinder
f_R	Roll gap model
f_s	Static mill stand model
F_{wrb}	Work roll bending force
g	Gravitational acceleration
h_0	Height of unloaded roll gap
h_{en}	Material entry thickness
h_{ex}	Material exit thickness
k_B	Feedback gain of AGC
k_0, m_1, m_2, m_3	Coefficients for yield stress
$K_{B,i}$	Bending stiffness of the beam i
k_{fm}	Yield stress
$K_{S,i}$	Shear stiffness of the beam i
L	Length of the finished strip
l_d	Length of the contact arc
m	Mass of the moving parts (upper roll stack)

*Corresponding author.

Email addresses: prinz@acin.tuwien.ac.at (K. Prinz), steinboeck@acin.tuwien.ac.at (A. Steinboeck), kugi@acin.tuwien.ac.at (A. Kugi)

Post-print version of the article: K. Prinz, A. Steinboeck, and A. Kugi, "Optimization-based feedforward control of the strip thickness profile in hot strip rolling", *Journal of Process Control*, vol. 64, pp. 100–111, 2018, ISSN: 0959-1524. DOI: 10.1016/j.jprocont.2018.02.001
The content of this post-print version is identical to the published paper but without the publisher's final layout or copy editing.

M_i	Bending moment of the beam i
N	Number of discretization elements
N_z	Number of discretization elements
p_{en}	Strip tension at entry side
p_{ex}	Strip tension at exit side
$p_h(z)$	Polynomial approximating the exit thickness
Q_i	Shear force of the beam i
q_c	Local contact force
q_{roll}	Local roll force
s_{wrs}	WR shifting position
T_{en}	Material entry temperature
u_R	Rolling velocity
v_i	Deflection of the beam i
w	Exit thickness wedge
x_h	HGC cylinder position
$\mathbf{\Phi}_k$, $\mathbf{\Gamma}_k$	Solution of linearized ODE
$\mathbf{A}$, $\mathbf{b}$	System of linearized static mill stand model
$\mathbf{A}_k$, $\mathbf{b}_k$	Linearized ODE
$\mathbf{u}$	Vector of inputs
$\mathbf{y}_k$	State vector for boundary value problem
δ_{bw}	Compression between WR and BR
δ_B	Displacement of the hydrodynamic bearing
δ_{wr}	Flattening of the WR
σ_{hex}	Standard deviation of the thickness error
φ	Degree of deformation
φ_i	Angle of rotation of the beam i
ξ_{cal}	Calibration offset of roll gap height

Subscripts and Superscripts

$_{AGC}$	Output of AGC
$_{br}$	Backup roll
$_{cal}$	Calibration parameter
$_{DS}$	Drive side
$_{en}$	Entry side of roll gap
$_{ex}$	Exit side of roll gap
$_{FF}$	Output of feedforward
$_{l}$	Lower roll
$_{opt}$	Output of optimization
$_{OS}$	Operator side
^{u}	Upper roll
$_{d}$	Desired values
$\bar{\ }$	Operating point
*	Optimal values
Δ	Difference to operating point
$\dot{\ }$	Time derivative
$\hat{\ }$	Estimated values
$\vert_A$	Operating point
$'$	Derivative with respect to x
†	Matrix pseudoinverse

1. Introduction

In hot strip rolling, a central objective is the production of strips with an accurate and uniform thickness. Therefore, at each mill stand of the tandem hot rolling mill considered in this paper, the strip thickness can be adjusted by hydraulic cylinders that move the upper roll stack. Additionally, the mill stands are equipped with a work roll bending system (WRB) to compensate for the bending deflection of the work rolls and to control the strip crown.

1.1. Literature review

The widely used automatic gauge controller (AGC) causes a non-zero steady-state control error of the strip exit thickness for any entry disturbance or deviation from its operating point because of its limited feedback gain, [3; 7; 10]. The disturbance feedforward control concept proposed in [24] estimates the strip temperature and thickness at upstream mill stands and adjusts the setpoint for the hydraulic cylinder position at downstream mill stands. This position adjustment is derived from a linearized model, where only the mean thickness value but not the lateral profile is considered. An additional cylinder position that is equal for both sides of the mill stand is used as control input (SISO FF). In [14], it is suggested to additionally use the bending force in feedforward control.

In other feedforward concepts, the additional hydraulic cylinder position is obtained based on an estimation of the yield stress of the strip material, [5; 11]. In [17; 18], the variations of rolling conditions, e. g., the measured roll force, are divided into variations caused by the roll eccentricities and those caused by strip temperature inhomogeneities. It is possible to identify and distinguish the root of these variations in the frequency domain because the distance between the skid marks and the revolution speed of the rolls are known.

The control concepts known from literature targeting the strip shape, including the flatness of the strip, are merely feedback control structures. In [2], the measurement from a downstream shape meter is used to control the strip flatness using an actuator influence matrix. This causes a dead time (transport delay) in the controlled plant. In fact, the distance between measurement and control input can be very large, like in tandem rolling, where the shape meter measurement is typically located several meters after the last mill stand. A model predictive control (MPC) approach is used in [2] to obtain the control inputs for each mill stand. The system synchronizes the control action to compensate for the transport delay of the strip. A MIMO control method for the strip flatness based on roll bending is discussed in [21].

Other research works, see, e. g., [8; 20], deal with finding the optimal interstand crowns. The aim is to prevent wavy edges and center buckles and to determine the control parameters for the Level 2 setup. These setup control parameters are constant within each strip and thus disregard inhomogeneities of the strip in longitudinal direction.

1.2. Motivation and objective of this paper

The main goal of this paper is to develop a thickness control strategy that realizes the desired target exit thickness profile over the complete length of the strip as accurately as possible. The deviation of the lateral exit thickness profile from a desired profile should be systematically minimized using all available control inputs,

Post-print version of the article: K. Prinz, A. Steinboeck, and A. Kugi, "Optimization-based feedforward control of the strip thickness profile in hot strip rolling", *Journal of Process Control*, vol. 64, pp. 100–111, 2018, ISSN: 0959-1524. DOI: 10.1016/j.jprocont.2018.02.001
The content of this post-print version is identical to the published paper but without the publisher's final layout or copy editing.

i. e., the hydraulic cylinder position of the backup rolls at both sides of the mill stand, operator and drive side, and the bending forces at both sides of the work rolls. The proposed concept is a multi-input multi-output feedforward (MIMO FF) controller that yields the optimal transient control inputs, and will be described in Section 4. To calculate the (expected) exit thickness profile for the measured disturbances, a mathematical model of the mill stand is required. The model presented in Section 2 uses well-known sub-models (Sims roll gap model, Hensel-Spittel material model, Hertzian contact model, Timoshenko beam model).

2. Mathematical model of the mill stand

In this section, a detailed mathematical model of a single mill stand of the considered tandem hot rolling mill is presented. This model is used for simulation and is validated based on measurement results from the real plant. Parts of this model serve as a basis for the control design given in Section 4.

The upper roll stack of the considered mill stand is outlined in Fig. 1. The mill stand consists of the upper and lower work roll (WR) and the upper and lower backup roll (BR). In the roll gap between the work rolls, the steel strip is deformed. The backup rolls reduce the bending deflection of the work rolls. The position of the upper BR is adjusted by two hydraulic cylinders, one at the drive side (DS) and one at the operator side (OS), to control the height of the roll gap. An important output of this model is the lateral exit thickness profile of the strip. For the thickness profile, the impact of the WRB system is significant, and the continuous variable crown shape (CVC) of the rolls, [25], the thermal crown and wear (TCW) profile of the rolls, [29; 1], and the local flattening of the rolls, [9], have to be considered. The roll gap crown is adjusted by axial movement of the CVC work rolls (WRS, work roll shifting). This shifting position is kept constant within each strip and thus is not a degree of freedom for control or optimization.

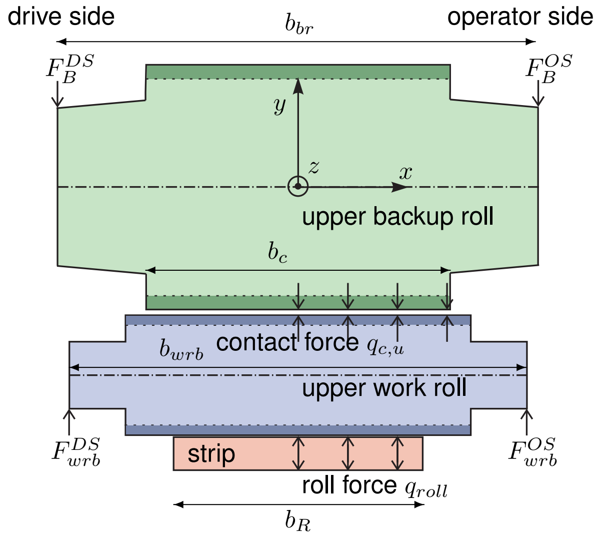

Figure 1: Section of upper roll stack (front view).

The main parts of the proposed model are the roll gap model, the static model of the deformation of the rolls and the mill housing, the dynamic model of the hydraulic gap actuators, and the existing subordinate controllers. These parts of the model are now described in detail, see also Fig. 2.

2.1. Roll gap model

The mathematical relation between the local roll force q_{roll}, the strip entry h_{en} and exit thickness h_{ex}, the strip tensions at the entry p_{en} and exit side p_{ex}, the rolling velocity u_R, and the yield stress k_{fm} of the strip material is referred to as roll gap model, which in general is written in the implicit form

$$f_R\big(q_{roll}, h_{en}, h_{ex}, p_{en}, p_{ex}, u_R, k_{fm}\big) = 0\,. \tag{1}$$

In the static mill stand model, the roll force q_{roll} depending on the exit thickness h_{ex} (and the other parameters) is required. For this purpose, q_{roll} is numerically computed. The rolling conditions in general vary over the strip width, so all the parameters in (1) depend on the lateral coordinate x, that is, the roll gap model is evaluated for $-\frac{b_R}{2} \leq x \leq \frac{b_R}{2}$ to obtain the distribution of the local roll force $q_{roll}(x)$.

According to [12], the mean yield stress k_{fm} of the strip material can be approximated in the form

$$k_{fm} = k_0 \mathrm{e}^{-m_1 T} \varphi^{m_2} \dot{\varphi}^{m_3}\,, \tag{2}$$

where T is the strip temperature, $\varphi = \ln\left(\frac{h_{ex}}{h_{en}}\right)$ is the deformation degree, and $\dot{\varphi}$ is its time derivative (the deformation rate). The mean deformation rate is proportional to the rolling velocity u_R, $\dot{\varphi} = \varphi \frac{u_R}{l_d}$ with the length of the contact arc l_d. The parameters k_0, m_1, m_2, and m_3 depend on the specific material and have to be identified for each strip material, e. g., by minimizing the deviation between the measured and the calculated roll force.

As roll gap models based on Sims' model [27] are commonly used in the steel industry, Sims' model is also applied in this paper but in an extended form that facilitates the consideration of the up- and downstream strip tension, [4]. However, the interface of (1) allows an easy substitution of this roll gap model with other models.

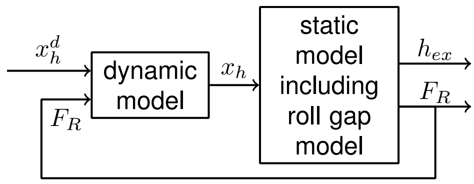

Figure 2: Structure of the dynamic simulation model.

Post-print version of the article: K. Prinz, A. Steinboeck, and A. Kugi, "Optimization-based feedforward control of the strip thickness profile in hot strip rolling", *Journal of Process Control*, vol. 64, pp. 100–111, 2018, ISSN: 0959-1524. DOI: 10.1016/j.jprocont.2018.02.001
The content of this post-print version is identical to the published paper but without the publisher's final layout or copy editing.

2.2. Static mill stand model

To model the bending deflection of the rolls, the four rolls are considered as Timoshenko beams [15; 19]. In the following, the abbreviation $(.)' = \frac{\mathrm{d}}{\mathrm{d}x}(.)$ is used. The differential equations for the deflection $v(x)$ along the direction y, the angle $\varphi(x)$ of rotation of the cross section, the bending moment $M(x)$, the shear force $Q(x)$, and the distributed load $q(x)$ read as

$$\begin{aligned} v_i' &= -\varphi_i + \frac{Q_i}{K_{s,i}} & \varphi_i' &= \frac{M_i}{K_{b,i}} \\ M_i' &= Q_i & Q_i' &= -q_i(v_{br,u}, v_{wr,u}, v_{wr,l}, v_{br,l}) \ . \end{aligned} \tag{3}$$

The variable i specifies the four rolls, upper BR and WR and lower WR and BR,

$$i \in \{br,u;\ wr,u;\ wr,l;\ br,l\} \ . \tag{4}$$

$K_{b,i}$ and $K_{s,i}$ are the bending and the shear stiffnesses of the rolls, respectively. They are calculated for the geometry of the rolls as outlined in Fig. 1, considering the different material properties of the soft core and the hard boundary layer of the rolls [28]. Together with the boundary conditions (see next paragraph), this results in a 16-dimensional nonlinear boundary value problem (4 equations for each roll). These beams are coupled by the load q_i, which depends on the roll force q_{roll} from Section 2.1 between the WR and the strip and the contact forces $q_{c,u}$ and $q_{c,l}$ between the WR and the BR,

$$\begin{aligned} q_{br,u} &= q_{c,u} & q_{wr,u} &= q_{roll} - q_{c,u} \\ q_{wr,l} &= -q_{roll} + q_{c,l} & q_{br,l} &= -q_{c,l} \ . \end{aligned} \tag{5}$$

For modeling the contact between WR and BR, the Hertzian theory of elastic contact is used. It gives $q_{c,u}$ and $q_{c,l}$ depending on $\delta_{bw,u}$ or $\delta_{bw,l}$, respectively, [13]. The compression δ_{bw} between two cylindrical bodies, i. e., the rolls that are in contact, is depending on v_i and is equal to

$$\begin{aligned} \delta_{bw,u} &= v_{wr,u} + c_{wr,u} - v_{br,u} + c_{br,u} \\ \delta_{bw,l} &= -v_{wr,l} + c_{wr,l} + v_{br,l} + c_{br,l} \ , \end{aligned} \tag{6}$$

where c_i is the total crown of the roll i (additional radius of the rolls) that includes the roll crown due to TCW, the manufactured CVC, and tapered roll ends. For the work rolls, the total local roll crown depends on the WRS s_{wrs}.

The link between the roll gap model (1) and the roll stack deflection model (3) is the exit thickness h_{ex}. It follows in the form

$$h_{ex} = h_0 + (v_{wr,u} - c_{wr,u}) - (v_{wr,l} + c_{wr,l}) + 2\delta_{wr} \ . \tag{7}$$

In (7), h_0 is the straight line connecting the roll gap height h_0^{DS} at the DS and h_0^{OS} at the OS,

$$h_0(x) = h_0^{DS} + \frac{h_0^{OS} - h_0^{DS}}{b_{br}} \left(x + \frac{b_{br}}{2} \right) \ . \tag{8}$$

As shown in Fig. 1, b_{br} is the distance between the HGC cylinders. The heights at the DS and at the OS depend on the cylinder positions x_h^{DS} and x_h^{OS}. In a calibration routine, the position of the HGC cylinders is recorded, when the work rolls are in contact and a defined force is applied. In this state, the roll gap heights are $h_0^{DS} = h_0^{OS} = 0$ and the calibration offsets ξ_{cal}^{DS} and ξ_{cal}^{OS} for the considered set of rolls are determined. So, the relations between the heights, h_0^{DS} and h_0^{OS}, and the cylinder positions, x_h^{DS} and x_h^{OS}, are

$$\begin{aligned} h_0^{DS} &= \xi_{cal}^{DS} - x_h^{DS} \\ h_0^{OS} &= \xi_{cal}^{OS} - x_h^{OS} \ . \end{aligned} \tag{9}$$

In (7), $h_0 - c_{wr,u} - c_{wr,l}$ is the height of the unloaded roll gap with the roll crowns $c_{wr,u}$ and $c_{wr,l}$ of the upper and lower work roll. With δ_{wr} in (7), the local flattening of the WR is considered. This local flattening is computed according to Boussinesq and Cerruti, [9; 13]. The pressure distribution along the arc of contact and the strip width is approximated by concentrated forces and the superposition of the corresponding deformation is computed.

The boundary value problem (3) requires 16 boundary conditions. The 8 boundary conditions for the WR are

$$\begin{aligned} Q_{wr,u}(-{}^{b_{wrb}}/_2 + s_{wrs}) &= -F_{wrb}^{DS} \\ Q_{wr,u}({}^{b_{wrb}}/_2 + s_{wrs}) &= F_{wrb}^{OS} \\ M_{wr,u}(\pm{}^{b_{wrb}}/_2 + s_{wrs}) &= 0 \\ Q_{wr,l}(-{}^{b_{wrb}}/_2 - s_{wrs}) &= F_{wrb}^{DS} \\ Q_{wr,l}({}^{b_{wrb}}/_2 - s_{wrs}) &= -F_{wrb}^{OS} \\ M_{wr,l}(\pm{}^{b_{wrb}}/_2 - s_{wrs}) &= 0 \ , \end{aligned} \tag{10}$$

where b_{wrb} is the distance between the bearings of the OS and the DS, and F_{wrb}^{DS} and F_{wrb}^{OS} are the bending forces applied by the hydraulic cylinders at the DS and at the OS. The parameter s_{wrs} is the shifting position of the WR. For $s_{wrs} > 0$, the upper WR is shifted by the distance s_{wrs} towards the OS, and the lower WR is displaced by $-s_{wrs}$ towards the DS. Hence, the bending forces are applied at the center of the bearings $x = \pm\frac{b_{wrb}}{2} \pm s_{wrs}$. The bending moment M_{wr} is zero at these points. Fig. 1 shows the upper roll stack with $s_{wrs} = 0$ and the applied forces. The remaining 8 boundary conditions for the BR are given at the position of the hydrodynamic bearings, $x = -\frac{b_{br}}{2}$ at the DS, and $x = \frac{b_{br}}{2}$ at the OS,

$$\begin{aligned} Q_{br,u}(-{}^{b_{br}}/_2) &= F_B^{DS}(v_{br,u}(-{}^{b_{br}}/_2) - \delta_{B,u}^{DS}) \\ Q_{br,u}({}^{b_{br}}/_2) &= -F_B^{OS}(v_{br,u}({}^{b_{br}}/_2) - \delta_{B,u}^{OS}) \\ M_{br,u}(\pm{}^{b_{br}}/_2) &= M_{br,l}(\pm{}^{b_{br}}/_2) = 0 \\ v_{br,l}(-{}^{b_{br}}/_2) &= -\delta_{B,l}^{OS} \\ v_{br,l}({}^{b_{br}}/_2) &= -\delta_{B,l}^{DS} \ . \end{aligned} \tag{11}$$

The force F_B as a function of the vertical position $v_{br,u}$ at the bearings $\pm{}^{b_{br}}/_2$ is obtained from a measured force-deflection curve of the mill stand frame. Additionally,

Post-print version of the article: K. Prinz, A. Steinboeck, and A. Kugi, "Optimization-based feedforward control of the strip thickness profile in hot strip rolling", *Journal of Process Control*, vol. 64, pp. 100–111, 2018, ISSN: 0959-1524. DOI: 10.1016/j.jprocont.2018.02.001
The content of this post-print version is identical to the published paper but without the publisher's final layout or copy editing.

in $\delta_{B,u}^{DS}$, $\delta_{B,u}^{OS}$, $\delta_{B,l}^{DS}$ and $\delta_{B,l}^{OS}$ the displacement of the hydrodynamic journal bearings of the backup rolls are included. This displacement, depending on the applied force F_B and the revolution speed of the BR, is taken from a lookup-table. This lookup-table is based on measurements of the displacement at reference forces and speeds and was provided by the plant operator.

A numerically efficient solution method for the boundary value problem (3), (10), (11) of the four Timoshenko beams is presented in Appendix A. In the following, the two outputs roll force $F_R = \int_{-\frac{b_R}{2}}^{\frac{b_R}{2}} q_{roll}\,\mathrm{d}x$ and exit thickness profile $h_{ex}(x)$ from (7) are used. As an abbreviation for this solution of the static mill stand model, we will write

$$\begin{aligned} h_{ex}(x) &= f_s\big(x_h^{DS}, x_h^{OS}, q_{roll}(.), F_{wrb}^{DS}, F_{wrb}^{OS}, s_{wrs}, u_R\big) \\ f_R\big(q_{roll}&, h_{en}, h_{ex}, p_{en}, p_{ex}, u_R, k_{fm}\big) = 0 \end{aligned} \tag{12}$$

for the rest of this paper.

The calculated profile $h_{ex}(x)$ of the model was validated by comparing it to the exit thickness profile measured by a downstream thickness measurement device. Fig. 3 shows the results for a representative strip for a certain longitudinal coordinate z of the strip. The agreement between the measurement and the model results is very satisfactory for most parts of the strip. Only at the strip edges, some small deviations in the range of up to 50 µm do occur. They are most likely due to the simplifications of the rolling conditions as the three-dimensional edge effects of the deformation are not considered. Since there is no control input that only acts at these edge zones, this model-plant mismatch is acceptable for a model that will be mainly used for control purposes. A comparison of several strips and over the complete length of the strips was made for validation, and resulted in a similar model accuracy, that is, less than 50 µm of maximum deviations of the strip profile.

2.3. Dynamic model of the hydraulic gap actuators

For simulation of the actual rolling process, a description of the dynamic behavior of the hydraulic actuators is needed, i. e., the differential equations for the pressures in the hydraulic cylinders, and the dynamics and characteristics of the servo valves. The hydraulic forces F_h^{DS} and F_h^{OS} applied by the HGC cylinders to move the upper roll stack is given by the pressure conditions in the cylinder chambers. The movement x_h^{DS} and x_h^{OS} of the upper roll stack with the mass m is described by the momentum balance

$$\begin{aligned} \frac{m}{2}\frac{\mathrm{d}^2}{\mathrm{d}t^2}x_h^{DS} &= F_h^{DS} - F_B^{DS} - \frac{F_{bal}}{2} + \frac{m}{2}g + F_f^{DS} \\ \frac{m}{2}\frac{\mathrm{d}^2}{\mathrm{d}t^2}x_h^{OS} &= F_h^{OS} - F_B^{OS} - \frac{F_{bal}}{2} + \frac{m}{2}g + F_f^{OS} \end{aligned} \tag{13}$$

including the hydraulic forces F_h^{DS} and F_h^{OS}, the bearing forces F_B^{DS} and F_B^{OS}, the balancing force F_{bal}, the gravitational force mg, and some frictional forces F_f^{DS} and F_f^{OS}. The latter may occur between the mill frame and the chocks of the roll bearings as well as in the hydraulic cylinders. These friction forces were identified in a measurement campaign. The bearing forces F_B^{DS} and F_B^{OS} are the outputs of the static mill stand model from the load of the upper BR of (11). These forces are obtained from the solution of the boundary value problem and they sum up the roll force F_R and the bending forces, see Fig. 1,

$$F_B^{DS} + F_B^{OS} = F_R + F_{wrb}^{DS} + F_{wrb}^{OS}\,. \tag{14}$$

2.4. Subordinate controllers

The positions x_h^{DS} and x_h^{OS} of the hydraulic cylinders are controlled by subordinate control loops according to [16], also referred to as HGC (hydraulic gap control). The reference signals of these HGC loops are the desired positions of the hydraulic cylinders $x_h^{DS,d}$ and $x_h^{OS,d}$, which are typically provided by the AGC [6; 23; 30]. In the AGC, the deviations Δ of the force and position measurements from their reference values are used to estimate the deviation of the average exit thickness

$$\Delta\hat{h}_{ex} = -\frac{\Delta x_h^{DS} + \Delta x_h^{OS}}{2} + \frac{\Delta F_R^{DS} + \Delta F_R^{OS}}{2c_m}\,, \tag{15}$$

where c_m is the mill modulus that is used for a linear approximation of the deformation of the mill stand $\frac{\Delta F_R^{DS}+\Delta F_R^{OS}}{2c_m}$. The estimation of $\hat{h}_{ex}$ is used in a proportional control with the feedback gain k_B

$$\Delta x_h^{agc} = k_B\left(\Delta\hat{h}_{ex} - \Delta h_{ex}^d\right) \tag{16}$$

for an additional cylinder position at both sides

$$\begin{aligned} x_h^{DS,d} &= \bar{x}_h^{DS} + \Delta x_h^{agc} \\ x_h^{OS,d} &= \bar{x}_h^{OS} + \Delta x_h^{agc}\,, \end{aligned} \tag{17}$$

added to the reference for the cylinder positions, $\bar{x}_h^{DS}$ and $\bar{x}_h^{OS}$, to compensate for the deflection of the mill stand. The AGC is typically used in industry for thickness control and will thus be used as a benchmark for the controller developed in this paper. Because the feedback of

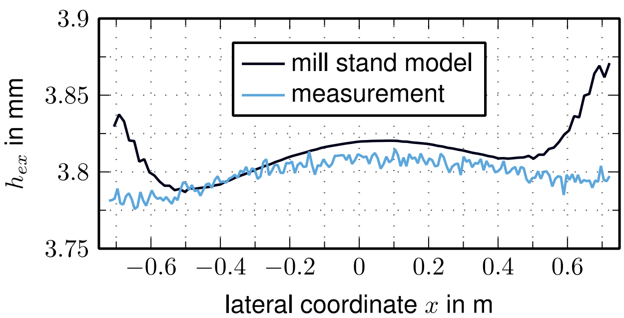

Figure 3: Comparison of the model and the measurement of the exit thickness profile at the last mill stand for a representative strip.

Post-print version of the article: K. Prinz, A. Steinboeck, and A. Kugi, "Optimization-based feedforward control of the strip thickness profile in hot strip rolling", *Journal of Process Control*, vol. 64, pp. 100–111, 2018, ISSN: 0959-1524. DOI: 10.1016/j.jprocont.2018.02.001
The content of this post-print version is identical to the published paper but without the publisher's final layout or copy editing.

the AGC (16) is proportional to the thickness error, disturbances like a varying strip temperature yield a non-zero steady-state control error, [23]. To systematically reduce this control error and to improve the control performance, SISO and MIMO feedforward control strategies are developed in the next sections.

3. Simple SISO feedforward control strategy

In this section, a simple approach of a linearized feedforward control strategy at the first mill stand is described. Similar methods have already been proposed in, e. g., [5; 11; 14; 24]. In the simulation scenarios presented in Section 6, the SISO feedforward controller will be compared to the proposed optimization-based MIMO feedforward controller (Section 4).

In the considered rolling process, the rolling conditions, i. e., the temperature and the entry thickness of the strip, as well as the rolling velocity, can vary over the strip length. These inputs influence the roll force and the yield stress, (1), (2). The entry inhomogeneities of the strip temperature and the strip thickness are measured by pyrometers and by a thickness measurement device, respectively, before the first mill stand in the considered tandem mill. The rolling velocity is known from the main drives of the WRs at each mill stand. The feedforward controller makes use of this information known ahead.

By linearizing the roll force model (1) and the material model for the yield stress (2), the expected roll force difference ΔF_R^{ff} from the operating point is obtained in the form

$$\Delta F_R^{ff} = \Delta h_{en} \frac{\partial F_R}{\partial h_{en}} + \Delta T_{en} \frac{\partial F_R}{\partial T_{en}} + \Delta u_R \frac{\partial F_R}{\partial u_R} \ . \tag{18}$$

The terms $\frac{\partial F_R}{\partial h_{en}}$, $\frac{\partial F_R}{\partial T_{en}}$, and $\frac{\partial F_R}{\partial u_R}$ are the scalar sensitivities of the roll force with respect to variations of the inputs. They are calculated numerically by central difference quotients from (1) and (2) at the operating point. The deviations Δh_{en}, ΔT_{en}, and Δu_R from their operating point are obtained from the measurements (in the lateral center of the strip). The expected roll force difference ΔF_R^{ff} from (18) causes a deflection $\frac{\Delta F_R^{ff}}{2c_m}$ of the mill stand, which can be compensated by an additional cylinder position

$$\Delta x_h^{ff} = \frac{\Delta F_R^{ff}}{2c_m} - \Delta h_{ex}^d \ , \tag{19}$$

where the same linearization of the mill stand deformation as in the thickness estimation (15) is used. The position Δx_h^{ff} is added to the reference position at the DS and the OS

$$\begin{aligned} x_h^{DS,ff} &= \bar{x}_h^{DS} + \Delta x_h^{ff} \\ x_h^{OS,ff} &= \bar{x}_h^{OS} + \Delta x_h^{ff} \ . \end{aligned} \tag{20}$$

Thus, the compensation Δx_h^{ff} of the (expected) mill stretch is symmetric.

The feedforward approach can be combined with the AGC to a two-degree-of-freedom controller as will be described in Section 5. The advantage of this SISO approach is that the implementation of (18) and (19) is simple and the required measurements of Δh_{en}, ΔT_{en}, and Δu_R are already available. However, the control law is based on the linearized roll gap model (18), which becomes inaccurate for larger deviations from the operating point. Additionally, the lateral exit thickness profile is not considered and the control input is symmetric for the DS and the OS. An asymmetric control input of the HGC cylinders is important for possibly occurring asymmetric rolling conditions, e. g., for wedge-shaped thickness profiles or for a strip rolled outside of the lateral center of the roll gap. In [22], an asymmetric feedforward approach was proposed. In the considered rolling mill, the WR bending forces F_{wrb} are also available as control inputs. In the next section, a more advanced approach of the feedforward controller is developed.

4. Optimization-based feedforward control strategy

The control strategy developed in the following is a feedforward compensation of measured or estimated disturbances from upstream entities using all available control inputs in a systematic way. The control inputs are the positions x_h^{DS} and x_h^{OS} of the hydraulic cylinders and the bending forces F_{wrb}^{DS} and F_{wrb}^{OS}, which are combined in the input vector

$$\mathbf{u} = \left[x_h^{DS}, x_h^{OS}, F_{wrb}^{DS}, F_{wrb}^{OS}\right]^{\mathrm{T}} \ . \tag{21}$$

The considered disturbances are the entry temperature profile $T_{en}(x,z)$ and the entry thickness profile $h_{en}(x,z)$ of the strip. For the design of the MIMO feedforward controller, these profiles are mapped to the strip cross section that is currently in the roll gap. The overall aim of the optimization-based control strategy is to achieve the desired exit thickness profile $h_{ex}^d(x)$ of the strip as accurately as possible.

4.1. Optimization problem

The deviation between the (predicted) lateral thickness profile $h_{ex}(x)$ and the desired profile $h_{ex}^d(x)$ is considered in the cost function of the optimization problem in the following form

$$e = \sqrt{\frac{1}{b_R - 2\tilde{b}} \int_{-\frac{b_R}{2}+\tilde{b}}^{\frac{b_R}{2}-\tilde{b}} \left(h_{ex}(x) - h_{ex}^d(x)\right)^2 \mathrm{d}x} \ . \tag{22}$$

The quadratic deviation of the profile is integrated and scaled, so that e represents a thickness. The integration domain ranges from $-\frac{b_R}{2}+\tilde{b}$ to $\frac{b_R}{2}-\tilde{b}$ with the width b_R of the strip and a user-defined constant $\tilde{b} \geq 0$. By means of

Post-print version of the article: K. Prinz, A. Steinboeck, and A. Kugi, "Optimization-based feedforward control of the strip thickness profile in hot strip rolling", *Journal of Process Control*, vol. 64, pp. 100–111, 2018, ISSN: 0959-1524. DOI: 10.1016/j.jprocont.2018.02.001
The content of this post-print version is identical to the published paper but without the publisher's final layout or copy editing.

$\tilde{b}$, the integration domain can be restricted to the relevant part of the strip and the edge zones can be excluded. To find the optimal control input, the cost function e is minimized,

$$\begin{aligned}
&\min_{\mathbf{u}} \quad e \\
&\text{s.t.} \quad h_{ex}(x) = f_s\big(x_h^{DS}, x_h^{OS}, q_{roll}(.), F_{wrb}^{DS}, F_{wrb}^{OS}, s_{wrs}, u_R\big) \\
&\qquad\quad f_R\big(q_{roll}, h_{en}, h_{ex}, p_{en}, p_{ex}, u_R, k_{fm}\big) = 0\;.
\end{aligned} \tag{23}$$

Additionally, the constraints

$$0 \le x_h^j \le x_h^{max}, \quad 0 \le F_{wrb}^j \le F_{wrb}^{max} \quad \forall j \in \{DS, OS\} \tag{24}$$

have to be considered. This optimization problem can be solved using standard algorithms, for instance the MATLAB command `fmincon`.

In the iterative optimization routine, the static mill stand model (12) has to be repeatedly solved and therefore the computational time associated with (23) is too high for a real-time implementation on a state-of-the-art hardware. This is why a computationally efficient approach is presented in the following subsection.

4.2. Numerically efficient solution of the optimization problem

In a first step, the mill stand model f_s is linearized in (23). For the linearization, a reasonable mill setup and suitable strip entry conditions are defined as operating point A. Here, the average values over the strip length are chosen for the point A, defined by

$$\begin{aligned}
&\bar{\mathbf{u}} = \left[\bar{x}_h^{DS}, \bar{x}_h^{OS}, \bar{F}_{wrb}^{DS}, \bar{F}_{wrb}^{OS}\right]^{\mathrm{T}}, \bar{s}_{wrs}, \bar{u}_R, \\
&\bar{h}_{ex}(x) = f_s\big(\bar{x}_h^{DS}, \bar{x}_h^{OS}, \bar{q}_{roll}(.), \bar{F}_{wrb}^{DS}, \bar{F}_{wrb}^{OS}, \bar{s}_{wrs}, \bar{u}_R\big) \\
&f_R\big(\bar{q}_{roll}, \bar{h}_{en}, \bar{h}_{ex}, \bar{p}_{en}, \bar{p}_{ex}, \bar{u}_R, \bar{k}_{fm}\big) = 0\;.
\end{aligned} \tag{25}$$

This yields the deviation $\Delta h_{ex}(x) = h_{ex}(x) - h_{ex}^d(x)$ at the grid points x_k, $k = 0, \ldots, N$. Summarizing these deviations in a vector, the linearization reads as

$$\begin{aligned}
\Delta\mathbf{h}_{ex} &= [\Delta h_{ex}(x_k)]_{k=0,\ldots,N}^{\mathrm{T}} = \Delta\bar{\mathbf{h}}_{ex} + \left.\frac{\partial \mathbf{f}_s}{\partial x_h^{DS}}\right|_A \Delta x_h^{DS} \\
&+ \left.\frac{\partial \mathbf{f}_s}{\partial x_h^{OS}}\right|_A \Delta x_h^{OS} + \left.\frac{\partial \mathbf{f}_s}{\partial F_{wrb}^{DS}}\right|_A \Delta F_{wrb}^{DS} + \left.\frac{\partial \mathbf{f}_s}{\partial F_{wrb}^{OS}}\right|_A \Delta F_{wrb}^{OS} \\
&+ \left.\frac{\partial \mathbf{f}_s}{\partial \mathbf{q}_{roll}}\right|_A \Delta\mathbf{q}_{roll} + \left.\frac{\partial \mathbf{f}_s}{\partial s_{wrs}}\right|_A \Delta s_{wrs} + \left.\frac{\partial \mathbf{f}_s}{\partial u_R}\right|_A \Delta u_R\;.
\end{aligned} \tag{26a}$$

The vector $\Delta\bar{\mathbf{h}}_{ex}$ contains the deviation between the exit thickness profile at the operating point A and the desired exit thickness, $\Delta\bar{h}_{ex}(x) = \bar{h}_{ex}(x) - h_{ex}^d(x)$. Additionally, the deviations from the operating point are denoted by $\Delta\mathbf{u} = \mathbf{u} - \bar{\mathbf{u}} = \left[x_h^{DS} - \bar{x}_h^{DS}, x_h^{OS} - \bar{x}_h^{OS}, F_{wrb}^{DS} - \bar{F}_{wrb}^{DS}, F_{wrb}^{OS} - \bar{F}_{wrb}^{OS}\right]^{\mathrm{T}}$ for the control input vector, $\Delta\mathbf{q}_{roll} = [q_{roll}(x_k) - \bar{q}_{roll}(x_k)]_{k=0,\ldots,N}^{\mathrm{T}}$ for the distribution of the roll force, $\Delta s_{wrs} = s_{wrs} - \bar{s}_{wrs}$ for the WR shifting position, and $\Delta u_R = u_R - \bar{u}_R$ for the rolling speed. Because the shifting position of the work rolls s_{wrs} is not changed during a roll pass, $\Delta s_{wrs} = 0$ and the term $\left.\frac{\partial \mathbf{f}_s}{\partial s_{wrs}}\right|_A \Delta s_{wrs}$ is omitted in the following.

This linearization of the mill stand model f_s is reasonable because the nonlinearity of this model is only weak. In contrast, the nonlinear roll gap model f_R is still used to obtain $\Delta\mathbf{q}_{roll}$. A comparison of the exit thickness of the linearized mill stand model with the full nonlinear model shows a good agreement for different variations of the system parameters. For this reason, the trajectories for the optimal control inputs $\mathbf{u}$ of the linearized mill stand model agree well with the inputs computed by the nonlinear optimization (23), see Fig. 9 in Section 6.

Using the abbreviations

$$\mathbf{A} = \left.\frac{\partial \mathbf{f}_s}{\partial \mathbf{u}}\right|_A = \left[\left.\frac{\partial \mathbf{f}_s}{\partial x_h^{DS}}\right|_A, \left.\frac{\partial \mathbf{f}_s}{\partial x_h^{OS}}\right|_A, \left.\frac{\partial \mathbf{f}_s}{\partial F_{wrb}^{DS}}\right|_A, \left.\frac{\partial \mathbf{f}_s}{\partial F_{wrb}^{OS}}\right|_A\right] \tag{26b}$$

$$\mathbf{b} = \Delta\bar{\mathbf{h}}_{ex} + \left.\frac{\partial \mathbf{f}_s}{\partial \mathbf{q}_{roll}}\right|_A \Delta\mathbf{q}_{roll} + \left.\frac{\partial \mathbf{f}_s}{\partial u_R}\right|_A \Delta u_R\;, \tag{26c}$$

(26a) is written as

$$\Delta\mathbf{h}_{ex} = \mathbf{A}\Delta\mathbf{u} + \mathbf{b}\;. \tag{26d}$$

Equation (26) facilitates a fast computation of $\Delta\mathbf{h}_{ex}$ because the nonlinear optimization problem (23) can be replaced by the quadratic program

$$\begin{aligned}
&\min_{\Delta\mathbf{u}} \quad \frac{1}{N + 1 - 2\frac{\tilde{b}}{b_R}N} \sum_{k=\frac{\tilde{b}}{b_R}N}^{N-\frac{\tilde{b}}{b_R}N} \Delta h_{ex}^2(x_k) \\
&\text{s.t.} \quad \Delta\mathbf{h}_{ex} = \mathbf{A}\Delta\mathbf{u} + \mathbf{b} \\
&\text{with} \quad \Delta\mathbf{u} = \left[\Delta x_h^{DS}, \Delta x_h^{OS}, \Delta F_{wrb}^{DS}, \Delta F_{wrb}^{OS}\right]^{\mathrm{T}}
\end{aligned} \tag{27}$$

if the optimal value $\Delta\mathbf{q}_{roll}^*$ is known. The problem (27) can be easily solved using the matrix pseudo-inverse

$$\Delta\mathbf{u}^* = -\mathbf{A}^\dagger\mathbf{b} \tag{28}$$

to get the optimal control input $\mathbf{u}^* = \bar{\mathbf{u}} + \Delta\mathbf{u}^*$. For restricting the part of the strip width that is considered in the optimization problem, as with $\tilde{b}$ in (22), the corresponding $\frac{\tilde{b}}{b_R}N$ first and last indexes of $\Delta\mathbf{h}_{ex}$ are omitted in (27). The value of $\frac{\tilde{b}}{b_R}N$ is round to integer. To obtain the corresponding optimal value $\Delta\mathbf{q}_{roll}^*$, (1), (26d) and (28) are

Post-print version of the article: K. Prinz, A. Steinboeck, and A. Kugi, "Optimization-based feedforward control of the strip thickness profile in hot strip rolling", *Journal of Process Control*, vol. 64, pp. 100–111, 2018, ISSN: 0959-1524. DOI: 10.1016/j.jprocont.2018.02.001
The content of this post-print version is identical to the published paper but without the publisher's final layout or copy editing.

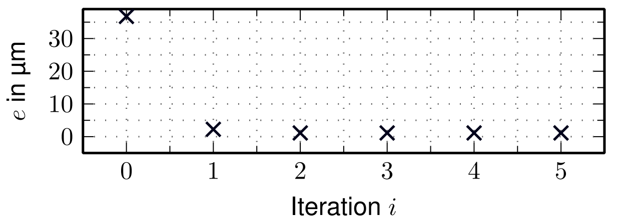

Figure 4: Evolution of the cost function e from (22) for five iterations of (29) for a representative optimization.

iteratively solved in the form

$$\mathbf{h}_{ex,i} = \mathbf{h}_{ex}^{d} + \mathbf{b}_i + \mathbf{A}\Delta\mathbf{u}_i \tag{29a}$$

$$\mathbf{q}_{roll,i} = f_R^{-1}\Big(\mathbf{h}_{en}, \mathbf{h}_{ex,i}, p_{en}, p_{ex}, u_R, \mathbf{k}_{fm}\Big) \tag{29b}$$

$$\mathbf{b}_{i+1} = \Delta\bar{\mathbf{h}}_{ex} + \frac{\partial \mathbf{f}_s}{\partial \mathbf{q}_{roll}}\left(\mathbf{q}_{roll,i} - \bar{\mathbf{q}}_{roll}\right) + \frac{\partial \mathbf{f}_s}{\partial u_R}\Delta u_R \tag{29c}$$

$$\Delta\mathbf{u}_{i+1} = -\mathbf{A}^{\dagger}\mathbf{b}_{i+1} \tag{29d}$$

$$i \leftarrow i+1\,, \tag{29e}$$

with the initial values $\mathbf{b}_0 = \Delta\bar{\mathbf{h}}_{ex}$, $\Delta\mathbf{u}_0 = \mathbf{0}$, and $i = 0$. In (29b), f_R^{-1} is the (numerical) solution of (1) for $\mathbf{q}_{roll}$. Fig. 4 shows a typical evolution of the cost function e from (22) for five iterations of (29). The iteration converges within 2 or 3 steps. Hence, a fixed maximum number of iterations turns out to be a good termination criterion for the above iterations.

In this linearized optimization approach, the constraints (24) are not considered. This is why a check of the optimal inputs obtained from (29d) is added after each step. If constraints are violated, the corresponding inputs are projected onto their limits and the iteration (29) is started again with the other inputs remaining for optimization.

The Jacobian $\frac{\partial \mathbf{f}_s}{\partial \mathbf{q}_{roll}}$ is numerically computed using the central difference quotient. Its values for a sample strip are shown in Fig. 5. In the same way, the sensitivities $\frac{\partial \mathbf{f}_s}{\partial \mathbf{u}}$ and $\frac{\partial \mathbf{f}_s}{\partial u_R}$ are numerically computed. The values $\mathbf{A} = \frac{\partial \mathbf{f}_s}{\partial \mathbf{u}}$ for a sample strip are shown in Fig. 6. Because $\mathbf{A}$ and $\frac{\partial \mathbf{f}_s}{\partial \mathbf{q}_{roll}}$ have to be calculated only once per strip, the computational costs associated with (29) are quite low, which allows a real-time implementation of this static optimization algorithm.

The proposed algorithm computes the control input $\mathbf{u}$ for a particular strip position in z-direction based on measurements of the inhomogeneities $T_{en}(x,z)$ and $h_{en}(x,z)$, and the actual velocity u_R. To obtain an optimal input $\mathbf{u}(z)$, the strip is discretized along the direction z and the algorithm (29) is applied to each grid point. The computation time of (29) is approximately 0.2 s for $N = 100$ discretization elements over the strip width b_R in the simulations with a standard PC in MATLAB. This means, the

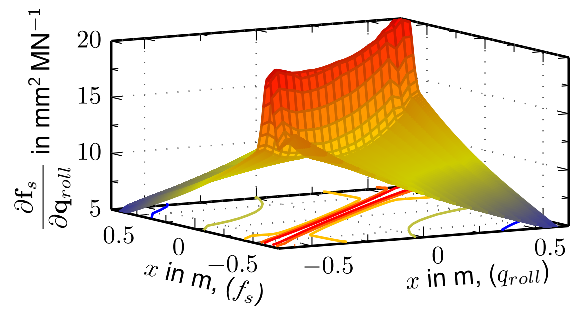

Figure 5: Jacobian $\frac{\partial \mathbf{f}_s}{\partial \mathbf{q}_{roll}}$ computed by central difference quotients for a representative strip.

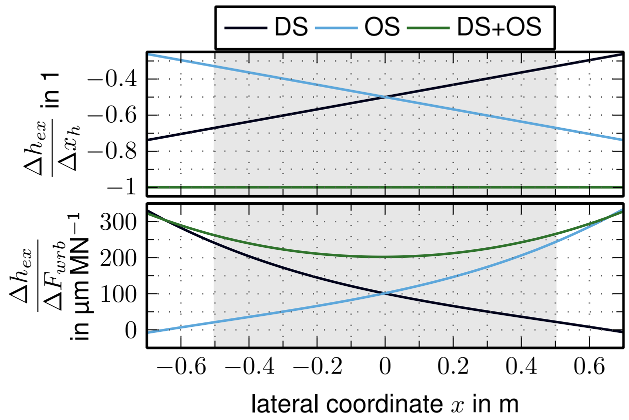

Figure 6: Sensitivities of the control inputs (components of $\mathbf{A}$) for a representative strip.

proposed optimization-based algorithm of (29) is real-time capable. The rolling time of one strip in a mill stand typically is about 90 s in the considered tandem rolling mill. This yields 450 discretization points of z, which corresponds to an average discretization distance of $\Delta z = 2$ m, or in the worst case $\Delta z = 4$ m if the strip is rolled with the maximum speed of $u_R = 20\,\mathrm{m\,s^{-1}}$, respectively. This discretization is sufficient to capture the variations of the entry properties $T_{en}(x,z)$ and $h_{en}(x,z)$, and the velocity u_R. As can be inferred from Fig. 9 and as will be discussed in Section 6.2, the result of the proposed solution strategy (29), which uses the linearized mill stand model, is almost identical to the optimal control input $\mathbf{u}(z)$ calculated with the nonlinear model (23). Numerical differences due to the linearization in the feedforward controller are not crucial for the resulting exit thickness because they are compensated by the feedback controller as discussed in Section 5.

5. Closed-loop control structure

The control strategy described in Section 4 yields a feedforward control input where the measurements of F_R and x_h are not used by the feedforward controller. This

Post-print version of the article: K. Prinz, A. Steinboeck, and A. Kugi, "Optimization-based feedforward control of the strip thickness profile in hot strip rolling", *Journal of Process Control*, vol. 64, pp. 100–111, 2018, ISSN: 0959-1524. DOI: 10.1016/j.jprocont.2018.02.001
The content of this post-print version is identical to the published paper but without the publisher's final layout or copy editing.

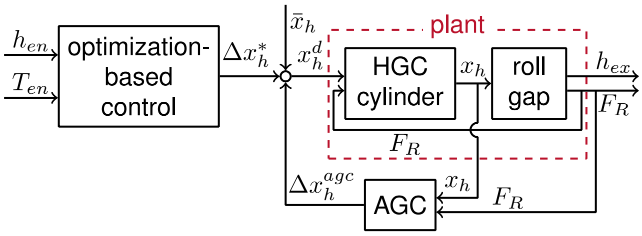

Figure 7: Two-degree-of-freedom controller structure with the AGC in the feedback loop combined with the (optimization-based) feedforward control strategy with the simulation model of Fig. 2 representing the industrial plant.

means, the resulting output thickness profile $h_{ex}(x)$ will be correct only if there is no model-plant mismatch and if the measurements of the strip entry temperature and strip entry thickness are exact. In the steel industry, an AGC loop is commonly used for thickness control, see also Section 2.4. The AGC calculates an additional (symmetric) cylinder position Δx_h^{agc} if there is a deviation between the estimated and the desired thickness, see (15), (16). When using the feedforward control concepts described in Section 3 and Section 4, the AGC loop can still be used as a feedback controller in a two-degree-of-freedom controller structure. The feedforward control input Δx_h^* from (29d) (or Δx_h^{ff} from (19)) is simply added to the AGC output Δx_h^{agc} as outlined in Fig. 7. If the feedforward controller is properly working, the control input of the AGC Δx_h^{agc} will be much smaller compared to a plant operating with the AGC only.

6. Simulation and measurement results

The control concept is compared to the conventional AGC in simulation studies using the validated simulation model described in Section 2. The static mill stand model from Section 2.2 including the roll gap model also serves as the basis for the control design.

The simulations cover a sample strip and the first mill stand. The control objective of the first mill stand is to compensate for entry inhomogeneities, and rolling speed variations, etc. such that the exit thickness of the first mill stand is preferably uniform in the longitudinal and lateral directions, that is, $h_{ex}^d(x, z) = \bar{h}_{ex}^d$.

6.1. Strip entry properties

To test the control design developed in Section 4, a sample strip with the inhomogeneities shown in Fig. 8 is considered. These inhomogeneities are taken directly from measurements in the real plant, i. e., the temperature is measured by a thermo-graphic camera and pyrometers, and the thickness profile is measured with a radiometric unit (infrared laser, x-ray). It is assumed that these measurements agree with the conditions how the strip enters the roll gap, e. g., a temperature change between the measurement and the first mill stand is not considered

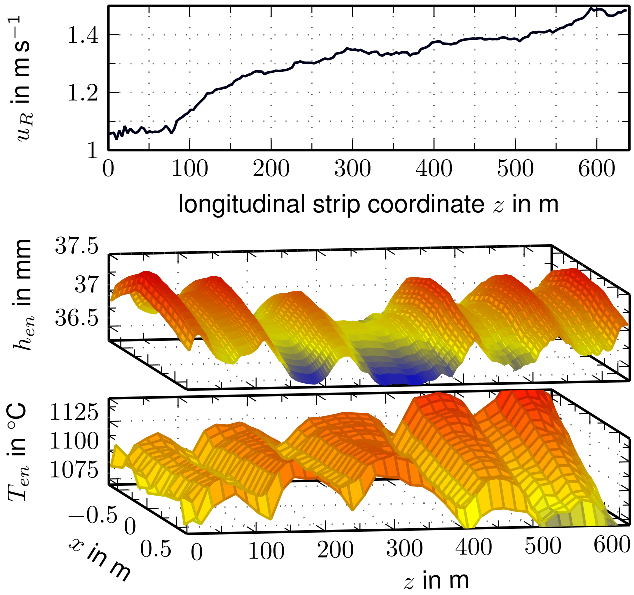

Figure 8: Measurements of the entry thickness profile h_{en}, the entry temperature profile T_{en}, and the rolling velocity u_R of the considered strip.

for the simulation. Fig. 8 shows the entry profiles for the strip thickness h_{en} and the temperature T_{en} as well as the rolling velocity u_R. The temperature skid marks originate from the pusher-type slab reheating furnace. Moreover, to discuss the influence of asymmetric rolling conditions, a temperature gradient T_{en} is assumed. Thus, starting at $z = 300$ m, the strip temperature at the DS is increased and at the OS decreased, respectively. Such asymmetric temperatures can stem from reheating the steel slab with one side close to the walls or door of the furnace and are added in the assumed strip temperature profile to show the behavior of the control approaches for asymmetries. These measurements suffice to assess the most significant features of the proposed controller. Other variations, e. g., of the strip tension, are not considered.

6.2. Simulation results

Fig. 9 shows the optimal control inputs $\mathbf{u}^*$ for the considered strip. The optimal control inputs Δx_h^* and F_{wrb}^* computed with the algorithm (29) based on the linearized mill stand model (solid lines) are almost identical to the optimal control inputs obtained from the nonlinear optimization (23) based on the full model (dashed lines). The additional cylinder position Δx_h^{ff} of the SISO feedforward controller according to (18) and (19) (purple dash-dotted line) is symmetric for the DS and the OS and plotted for comparison reasons. The WR bending forces are constant for the SISO feedforward controller. At the colder zones of the strip, the expected roll forces are higher, and therefore the feedforward controller requests an additional position Δx_h^* and higher bending forces ΔF_{wrb}^*. The

Post-print version of the article: K. Prinz, A. Steinboeck, and A. Kugi, "Optimization-based feedforward control of the strip thickness profile in hot strip rolling", *Journal of Process Control*, vol. 64, pp. 100–111, 2018, ISSN: 0959-1524. DOI: 10.1016/j.jprocont.2018.02.001
The content of this post-print version is identical to the published paper but without the publisher's final layout or copy editing.

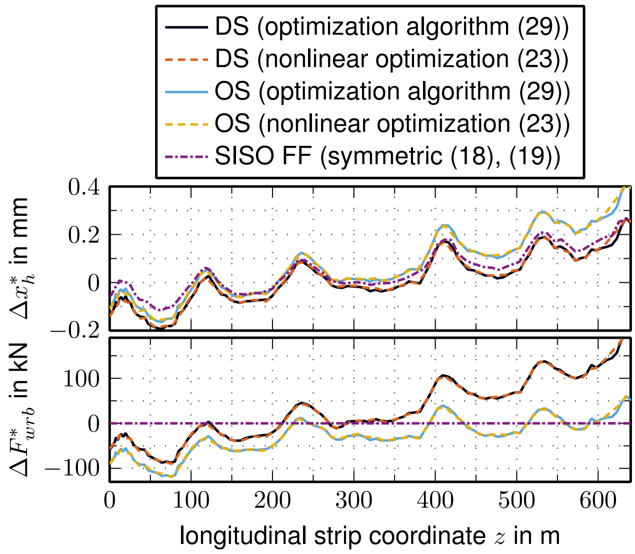

Figure 9: Optimal control inputs for the considered sample strip. Comparison of $\mathbf{u}^*$ computed with the algorithm (29) based on the linearized mill stand model (solid lines), with the nonlinear optimization (23) based on the full model (dashed lines), and the symmetric SISO FF (18), (19).

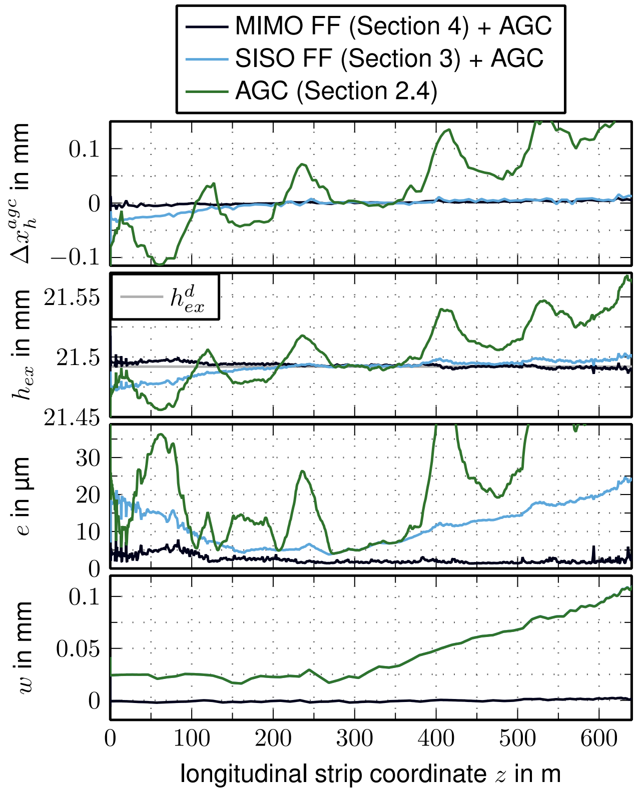

Figure 10: Simulation results for the optimal MIMO feedforward controller and a SISO feedforward controller with the feedforward control inputs from Fig. 9 compared to a standard AGC with the nominal plant.

increasing asymmetry of T_{en} requires asymmetric control inputs, that is, $\Delta x_h^{DS,*}$ and $\Delta x_h^{OS,*}$, and $\Delta F_{wrb}^{DS,*}$ and $\Delta F_{wrb}^{OS,*}$ are diverging to the end of the strip.

Fig. 10 shows the simulation results of 3 control approaches: the results of the optimal feedforward controller (MIMO FF) from Section 4 (black line) and the simple symmetric SISO feedforward controller from Section 3 (blue line), both with the AGC in the feedback loop in a two-degree-of-freedom controller structure, are compared to the results of a standard AGC (green line). In the optimization-based MIMO and the SISO feedforward control, the control action mainly comes from the feedforward part whereas the output of the AGC is rather small because there is nearly no model-plant mismatch. The feedforward control inputs Δx_h^* compared to the feedback control inputs Δx_h^{agc} are dominant. The figure also shows the mean exit thicknesses h_{ex} for all 3 control approaches. The aggregated error e as defined in (22) and the wedge-shape of the strip (the difference of $h_{ex}(x)$ between the DS and the OS) are shown in the bottom of Fig. 10. The desired exit thickness profile $\bar{h}_{ex}^d$ after the first mill stand is assumed constant over the strip width and length. This desired profile is best achieved by the optimization-based MIMO FF controller. As the standard AGC controller is a proportional feedback controller, the entry inhomogeneities cannot be completely compensated and the exit thickness still shows the skid marks.

For the SISO feedforward approach, the average exit thickness h_{ex} is quite accurate and superior compared to the pure AGC. The skid marks are largely compensated but small deviations can occur due to the linearization in (18), e. g., in the first part of the strip. The asymmetric rolling conditions due to the asymmetric temperature in the second half of the strip cannot be counteracted with the symmetric control input Δx_h^{ff}. Although the mean strip thickness h_{ex}^d is still equal to the desired exit thickness h_{ex}^d, there is a rising error e of the thickness profile due to the wedge shape w of the strip. The exit thickness wedge w (thickness difference between DS and OS edges of the strip) is the same for the SISO FF (blue lines) and the pure AGC (green lines) because both give symmetric control inputs. Even a small thickness wedge can lead to camber shape and to lateral strip movement, [26]. With the optimization-based MIMO feedforward control (black lines), those wedge-shapes are avoided and the error e is almost constant over the strip length. The aggregated error e is not exactly zero because there are remaining deviations between the thickness profile $h_{ex}(x)$ and the desired profile $h_{ex}^d(x)$. This is mainly because there are only four (scalar) control inputs $\mathbf{u}$ used to control the thickness $h_{ex}(x)$ (or the load $q_{roll}(x)$) that is distributed over x.

The simulated profiles in lateral x-direction at $z = 400$ m are shown in Fig. 11. In this figure, the gray shaded area represents the integration domain $\left[-\frac{b_R}{2}+\tilde{b}, \frac{b_R}{2}-\tilde{b}\right]$ in the cost function (22). For these results, $\tilde{b} = 0.15b_R$ was used. The exit thickness profile of the optimization-based approach (black line) in the gray area, is almost identi-

Post-print version of the article: K. Prinz, A. Steinboeck, and A. Kugi, "Optimization-based feedforward control of the strip thickness profile in hot strip rolling", *Journal of Process Control*, vol. 64, pp. 100–111, 2018, ISSN: 0959-1524. DOI: 10.1016/j.jprocont.2018.02.001
The content of this post-print version is identical to the published paper but without the publisher's final layout or copy editing.

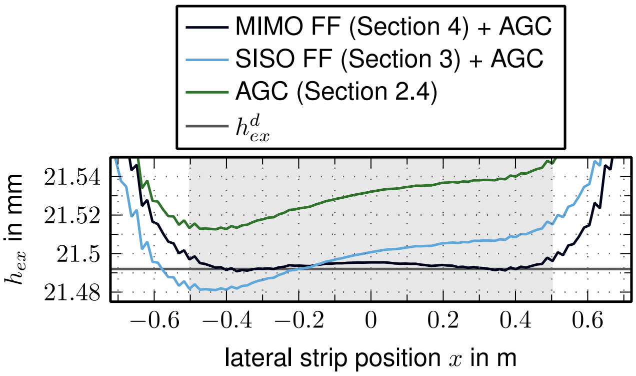

Figure 11: Exit thickness profiles at $z = 400\,\mathrm{m}$ for the three control approaches.

cal the desired exit thickness h_{ex}^d. For the SISO FF and the AGC, the exit thickness profiles are asymmetric because there is a wedge shape. However, for SISO FF, the mean exit thickness is very close the desired exit thickness, whereas for the pure AGC, there is a larger deviation.

6.3. Simulation results with model-plant mismatch

To analyze the robustness of the control concept against model-plant mismatches, the parameters of the simulation model were modified. For the results shown in Fig. 12, the exponent m_1 for the temperature T in (2) was increased by 10 %. As the optimal control inputs $\mathbf{u}^*$ are calculated based on nominal parameters, they are the same as in Fig. 9. Here, the exit thicknesses h_{ex} of both feedforward approaches differ from the desired thickness. Hence, the feedback from the AGC slightly improves the results, but there is a remaining error that is almost constant. However, these control concepts are still superior to the standard AGC. The constant control error could be easily reduced by adding a further integral feedback action. This could be done either in the AGC control law itself (16) or directly by a monitor thickness controller using the measured exit thickness.

6.4. Implementation and test in the real plant

In this section, first measurement results of the simple SISO feedforward control strategy according to Section 3 at the first mill stand of the considered finishing mill at voestalpine in Linz, Austria, are shown. Compared to (18), the rolling velocity u_R is not considered,

$$\Delta F_R^{ff} = \Delta h_{en} \frac{\partial F_R}{\partial h_{en}} + \Delta T_{en} \frac{\partial F_R}{\partial T_{en}} \tag{30}$$

is used. The scalar sensitivities $\frac{\partial F_R}{\partial h_{en}}$ and $\frac{\partial F_R}{\partial T_{en}}$ are used for the implementation in the industrial plant. These sensitivities are well known by the plant operator for the different materials. The scalar feedforward control action is obtained using (19) with (30).

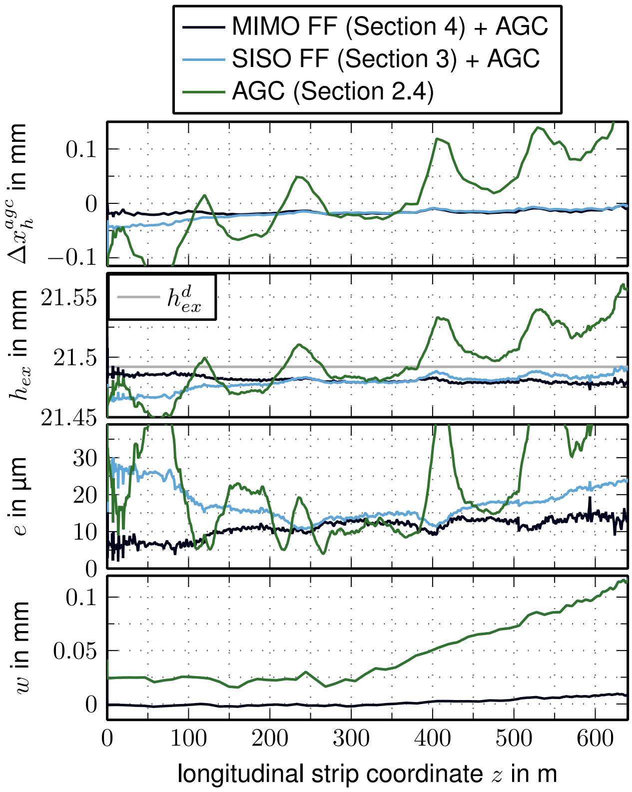

Figure 12: Simulation results for the optimal MIMO feedforward controller and a SISO feedforward controller with the feedforward control inputs from Fig. 9 compared to a standard AGC with a model-plant mismatch (10 % error of m_1 from (2)).

In this first step, the expected variations of the roll force ΔF_R^{ff} are calculated in the feedforward controller using the measured differences from the operating point of the entry thickness Δh_{en} and of the entry temperature ΔT_{en} of the strip. These measurements represent the average over the strip width, that is, the lateral profile is not considered so far. The entry thickness Δh_{en} is estimated at the last rolling pass of the roughing mill using (15). The temperatures of the upper and the lower surface of the strip are measured by two pyrometers before the first mill stand and then averaged. Since the measurements are far enough from the first mill stand, the calculation of the evolution of Δx_h^{ff} for one strip is available before the head end enters the first mill stand and the feedforward control input could be disabled in case of implausible shape. The feedforward control input is applied to the existing AGC loop as outlined in Section 5.

The strip velocity or other variations that influence the rolling process are not considered in this preliminary implementation. This means, this compensation of the inhomogeneities of the temperature and the entry thickness is in particular suitable for strips that are preheated in a pusher-type furnace that exhibit pronounced skid marks.

Post-print version of the article: K. Prinz, A. Steinboeck, and A. Kugi, "Optimization-based feedforward control of the strip thickness profile in hot strip rolling", *Journal of Process Control*, vol. 64, pp. 100–111, 2018, ISSN: 0959-1524. DOI: 10.1016/j.jprocont.2018.02.001
The content of this post-print version is identical to the published paper but without the publisher's final layout or copy editing.

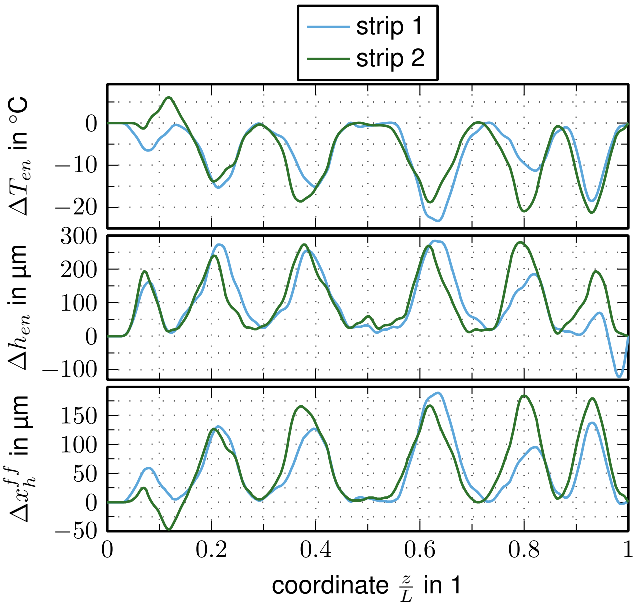

Figure 13: Measurement results from an industrial finishing mill for the entry properties of the strip used in the symmetric linearized SISO feedforward controller.

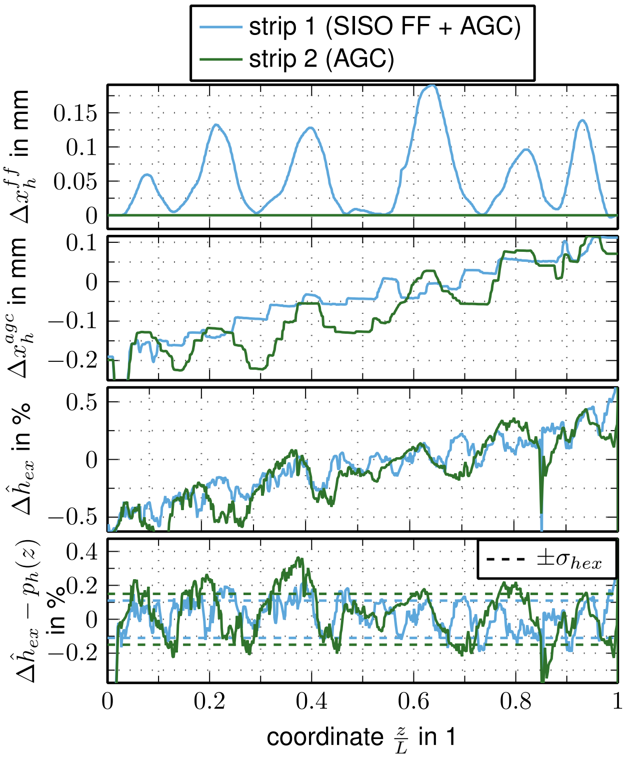

Figure 14: Measurement results from the first mill stand of an industrial finishing mill with (blue lines) and without (green lines) the symmetric linearized SISO feedforward controller with the variations of the strip entry temperature and thickness according to Fig. 13.

6.5. Measurement results

Fig. 13 shows the variations of the measured entry thicknesses and entry temperatures of two representative strips. The longitudinal coordinate z of the strips is normalized since the strips have different lengths L. The temperature profiles of the two strips exhibit typical skid marks caused by non-uniform reheating conditions in the pusher-type slab reheating furnace. Consequently, thickness variations occur at the roughing mill. The associated longitudinal thickness profile of the strips entering the first mill stand are also shown in Fig. 13. The bottom of Fig. 13 shows the additional position Δx_h^{ff}, that is the output of the feedforward control law (30). The feedforward control was added to the control input only for the first strip (blue lines) but the output Δx_h^{ff} was calculated for both strips. When comparing the control approaches, it must be kept in mind that strips are never completely identical. They can differ in their material properties, heating conditions, desired geometry, and rolling conditions, etc. The two strips shown in Fig. 13 are consecutively produced at the finishing mill.

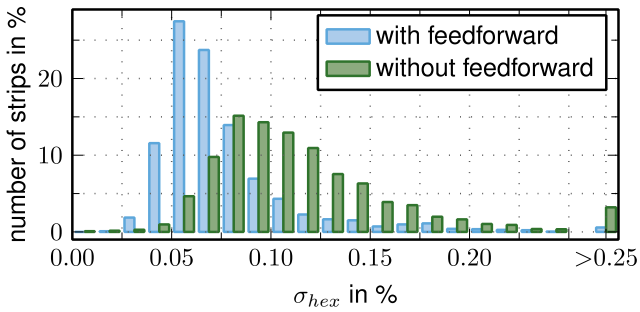

Figure 15: Statistical evaluation of the standard deviation (31) of the exit thickness from the first mill stand of an industrial finishing mill with (blue bars, 2250 strips) and without (green bars, 3200 strips) the symmetric linearized SISO feedforward controller.

In Fig. 14, the strip with pure AGC (green lines) is compared to the strip with active SISO feedforward control (blue lines). The figure shows the applied position Δx_h^{ff}, the additional position of the feedback AGC Δx_h^{agc}, and the estimated strip thickness $\Delta \hat{h}_{ex}$ after the first mill stand. At the bottom of Fig. 14, a first-order polynomial is subtracted from the estimated thickness $\hat{h}_{ex}$. The axis of the exit thickness deviation $\Delta \hat{h}_{ex}$ in the figure is the ratio to the nominal exit thickness after the first mill stand in %. In Fig. 14, the behavior of a properly working two-degree-of-freedom controller can be observed. The control input of the feedback controller (the AGC, Δx_h^{agc}) is smaller when it is combined with the feedforward controller. Since in this implementation only the entry thickness and the temperature of the strips are considered by the feedforward controller (as so decided by the plant operator), there is a remaining rise of the exit thickness that is due to the velocity speed up. Moreover, the cool-down of the strip between the temperature sensor and the rolling mill is not considered by the feedforward controller. The colder strip tail end causes higher roll forces and hence a rise of the exit thickness as well. The contin-

Post-print version of the article: K. Prinz, A. Steinboeck, and A. Kugi, "Optimization-based feedforward control of the strip thickness profile in hot strip rolling", *Journal of Process Control*, vol. 64, pp. 100–111, 2018, ISSN: 0959-1524. DOI: 10.1016/j.jprocont.2018.02.001
The content of this post-print version is identical to the published paper but without the publisher's final layout or copy editing.

uous increase of the estimated exit thickness $\Delta \hat{h}_{ex}$ is observed for both strips of Fig. 14, and is thus masked out by subtracting the first-order polynomial $p_h(z)$. The variations due to the skid marks almost vanish for the first strip with feedforward controller (blue lines). For the strip without any feedforward control action (green lines), the skid marks can still be seen in the signals Δx_h^{agc} and $\Delta \hat{h}_{ex}$. For this strip, only the AGC control law (16) was active. These results from an industrial application confirm the feasibility of the proposed feedforward control concept.

The feedforward control strategy was also tested with other strips. The behavior shown in Fig. 14 is representative for these strips. The standard deviation σ_{hex} of the remaining thickness deviations $\Delta \hat{h}_{ex} - p_h(z)$ over the strip length is used as an aggregate measure of the accuracy of the exit thickness,

$$\sigma_{hex} = \sqrt{\frac{1}{N_z - 1} \sum_{l=1}^{N_z} \left(\Delta \hat{h}_{ex}(z_l) - p_h(z_l) \right)^2} \qquad (31)$$

with the number of points N_z along the length of the strip. The standard deviations for the two strips are shown as dashed lines in Fig. 14. The standard deviation σ_{hex} was calculated for 2250 other strips rolled with the feedforward controller and for 3200 strips with pure AGC. Fig. 15 shows the frequency distribution of these standard deviations for both strategies, strips with active feedforward in blue bars and without feedforward (with AGC only) in green bars. This demonstrates that σ_{hex} is significantly lower with the feedforward strategy (mean value $0.077\,\%$) than without feedforward compensation of the skid marks (mean value $0.118\,\%$). The number of strips with large deviations of $\hat{h}_{ex}$ is drastically reduced with the feedforward approach of (19) and (30).

In the next step of the realization of the proposed feedforward control strategies, the rolling velocity will also be considered in the feedforward controller. Since the measurement results for the first mill stand agree well with the expectations from the simulation results for the linearized feedforward control strategy, it is also reasonable that the more complex feedforward strategies developed in this paper will work well, and will further improve the thickness control, in particular also in terms of the lateral thickness profile.

The measurement results obtained so far clearly validate the proposed feedforward concept and encourage the implementation of more features of the proposed feedforward strategies. The accuracy of the exit thickness after the first mill stand is improved if the variations of the entry thickness and entry temperature are compensated. Therefore, it is planned to implement the feedforward strategy also at consecutive mill stands to improve the quality of the finished strip.

7. Conclusions

In this paper, SISO and optimal MIMO feedforward control strategies to compensate for the measured incoming inhomogeneities of a strip at the first mill stand in a tandem hot rolling mill are discussed. The thickness profile is optimized using all available control inputs, i. e., the cylinder positions and the bending forces at the drive side and at the operator side. Linearizing the mill stand model (but not the roll gap model) lead to an iterative quadratic optimization problem, which can be solved in a computationally efficient way and thus facilitate real-time control. Simulation results show a significant benefit compared to conventional AGC concept. Thickness fluctuations due to skid marks are practically avoided and, even in case of a constant model-plant mismatch, there is only a constant error over the strip length, which can be corrected by adding a simple integral feedback action.

For this paper, it was assumed that the desired exit thickness of the first mill stand is uniform over the width and the length of the strip. Therefore, at the following mill stands, only the remaining temperature inhomogeneities have to be considered for feedforward optimization. As suggested in [24], it could also be useful to overcompensate the temperature at one mill stand such that both the exit thickness and the roll force are constant at the following mill stand. In the future research, the model will be adapted, in particular the material parameters of (2) could be estimated based on measurements at the mill stands. These parameters should then be used at subsequent mill stands to further improve the accuracy of the exit thickness profile. A feedforward control concept for the whole tandem mill including the loopers between the mill stands is another topic of future research.

Appendix A. Numerically efficient solution of the boundary value problem

For a numerically efficient solution of the boundary value problem stated in Section 2.2, a tailor-made numerical solver was developed. The general idea of this solver is to make use of the fact that the ODE (3) is only weakly nonlinear. Basically, the ODE is locally linearized, and with the exact solution of the linearized system of equations, a new starting point for the linearization is found iteratively. This approach for solving the boundary value problem is described in detail in the next paragraph.

At the ends of the rolls, $|x| > \frac{b_c}{2}$, there is neither a contact between WR and BR nor between WR and the strip. Hence, $q = 0$ holds in this region, (3) is linear, and an analytical solution of (3) can be readily found. The boundary conditions (10) and (11) are replaced by boundary conditions at $x = \pm\frac{b_c}{2}$. Within these boundaries, the nonlinear boundary value problem is numerically solved. Therefore, the ODEs are evaluated at $N + 1$ discrete points x_k, $k = 0, \ldots, N$ in x-direction starting with a reasonable initial value for the 16 states $\mathbf{y}_0 = [v_{i,0}, \varphi_{i,0}, M_{i,0}, Q_{i,0}]^{\mathrm{T}}$ at

Post-print version of the article: K. Prinz, A. Steinboeck, and A. Kugi, "Optimization-based feedforward control of the strip thickness profile in hot strip rolling", *Journal of Process Control*, vol. 64, pp. 100–111, 2018, ISSN: 0959-1524. DOI: 10.1016/j.jprocont.2018.02.001
The content of this post-print version is identical to the published paper but without the publisher's final layout or copy editing.

$x = x_0 = -\frac{b_c}{2}$ and ending at $x = x_N = \frac{b_c}{2}$, with i according to (4). After solving this initial value problem, using, e. g., a Runge-Kutta method, the solution $\mathbf{y}_k$ at each position x_k with $k = 0, \ldots, N-1$ is linearized in the form

$$\frac{\partial \mathbf{y}}{\partial x} \approx \mathbf{A}_k \mathbf{y} + \mathbf{b}_k \ , \quad x_k < x \leq x_{k+1} \ , \tag{A.1}$$

that is, a linear order Taylor series, where $\mathbf{A}_k$ represents the Jacobian of (3) at x_k. Using the matrix exponential of $\mathbf{A}_k$, the discrete solution formula reads as

$$\mathbf{y}_{k+1} = \mathbf{\Phi}_k \mathbf{y}_k + \mathbf{\Gamma}_k \ , \quad k = 0, \ldots, N-1 \tag{A.2}$$

with

$$\mathbf{\Phi}_k = \exp\left(\mathbf{A}_k \left(x_{k+1} - x_k\right)\right) \tag{A.3a}$$

$$\mathbf{\Gamma}_k = \int_{x_k}^{x_{k+1}} \mathbf{b}_k \exp\left(\mathbf{A}_k \left(x_{k+1} - \tau\right)\right) \mathrm{d}\tau \ . \tag{A.3b}$$

Recursive insertion yields

$$\begin{aligned} \mathbf{y}_k = & \underbrace{\sum_{j=0}^{k-2} \mathbf{\Phi}_{k-1} \mathbf{\Phi}_{k-2} \ldots \mathbf{\Phi}_{j+1} \mathbf{\Gamma}_j + \mathbf{\Gamma}_{k-1}}_{\tilde{\mathbf{\Gamma}}_k} \\ & + \underbrace{\mathbf{\Phi}_{k-1} \mathbf{\Phi}_{k-2} \ldots \mathbf{\Phi}_0}_{\tilde{\mathbf{\Phi}}_k} \mathbf{y}_0 \ , \qquad k = 0, \ldots, N \ , \end{aligned} \tag{A.4}$$

that is, an affine equation in the initial value $\mathbf{y}_0$.

Using $\mathbf{F}(\mathbf{y}_0, \mathbf{y}_N)$ for the 16 boundary conditions (10), (11) and inserting (A.4) yields

$$\mathbf{F}(\mathbf{y}_0, \mathbf{y}_N) = \mathbf{F}(\mathbf{y}_0, \tilde{\mathbf{\Phi}}_N \mathbf{y}_0 + \tilde{\mathbf{\Gamma}}_N) = \mathbf{0} \ , \tag{A.5}$$

a set of 16 nonlinear equations. They are solved for $\mathbf{y}_0$. With this new initial value $\mathbf{y}_0$, the values $\mathbf{\Phi}_k$ and $\mathbf{\Gamma}_k$ can be iteratively computed and the whole procedure can be repeated until the desired accuracy is obtained. This approach of linearizing the ODEs is computationally efficient and is suitable for the boundary value problem (3) because this is only weakly nonlinear. With a reasonable initial value $\mathbf{y}_0$, a sufficiently accurate solution can be found within two or three iterations. A very good initial value is the solution of a previous evaluation of the static mill stand model. When simulating the rolling of a strip with varying coordinate z, the previous result is suitable because the rolling conditions are just slowly changing. This initial solution is also directly used for the linearization (A.1), that is, the Runge-Kutta method is used for the very first solution of the ODE (3) only. Compared to a standard MATLAB solver for boundary value problems as `bvp4c`, the computation times could be improved by a factor of 10 below 1 s for $N = 200$ discretization points over the width b_c.

Acknowledgements

The financial support from the Austrian Federal Ministry for Digital, Business and Enterprise, and the National Foundation for Research, Technology and Development and voestalpine Stahl GmbH is gratefully acknowledged.

References

[1] M. Abbaspour and A. Saboonchi. Work roll thermal expansion control in hot strip mill. *Applied Mathematical Modelling*, 32(12):2652–2669, 2008.

[2] A. Bemporad, D. Bernardini, F. A. Cuzzola, and A. Spinelli. Optimization-based automatic flatness control in cold tandem rolling. *Journal of Process Control*, 20:396–407, 2010.

[3] T. S. Bilkhu. Hot strip mill gauge control. In *UKACC International Conference on Control*, pages 150–155, Coventry, UK, 2010.

[4] D. Bland and H. Ford. The calculation of roll force and torque in cold strip rolling with tensions. *Proceedings of the Institution of Mechanical Engineers*, 159:144–163, 1948.

[5] C.-C. Cheng, L.-Y. Hsu, Y.-L. Hsu, and P.-T. Chen. Simulation and analysis of feedforward automatic gauge control for a hot strip finishing mill. *Advanced Materials Research*, 230–232:471–475, 2011.

[6] I. J. Ferguson and R. F. De Tina. Modern hot-strip mill thickness control. *IEEE Transactions on Industry Applications*, 22(5):934–940, 1986.

[7] V. Ginzburg. *High-Quality Steel Rolling*. CRC Press, New York, 1993.

[8] R. M. Guo. Optimal profile and shape control of flat sheet metal using multiple control devices. *IEEE Transactions on Industry Applications*, 32(2):449–457, 1996.

[9] A. Hacquin, P. Montmitonnet, and J. Guillerault. A three-dimensional semi-analytical model of rolling stand deformation with finite element validation. *European Journal of Mechanics, A/Solids*, 17:79–106, 1998.

[10] G. Hearns and M. J. Grimble. Robust multivariable control for hot strip mills. *Iron and Steel Institute of Japan (ISIJ) International*, 40(10):995–1002, 2000.

[11] R. Heeg, T. Kiefer, A. Kugi, O. Fichet, and L. Irastorza. Feedforward control of plate thickness in reversing plate mills. *IEEE Transactions on Industry Applications*, 43(2):386–394, 2007.

[12] A. Hensel and T. Spittel. *Kraft- und Arbeitsbedarf bildsamer Formgebungsverfahren*. VEB Deutscher Verlag für Grundstoffindustrie, Leipzig, 1978.

[13] K. Johnson. *Contact Mechanics*. Cambridge University Press, Cambridge, 1985.

[14] G. Keintzel, M. Schoisswohl, P. Vorstandlechner, K. Aistleitner, and R. Schneeweis. Advanced control methods in rolling applications. In *Proceedings of the 33rd IEEE IAS Annual Meeting*, volume 3, pages 2263–2269, St. Louis, USA, 1998.

[15] T. König, A. Steinboeck, and A. Kugi. Online calibration of a mathematical model for the deflection of a rolling mill. In *Proceedings of Rolling 2013*, page 12, Venice, Italy, 2013.

[16] A. Kugi, K. Schlacher, and R. Novak. Nonlinear control in rolling mills: A new perspective. *IEEE Transactions on Industry Applications*, 37(5):1394–1402, 2001.

[17] Y. K. Lee, Y. J. Jang, and S. W. Kim. Adaptive feed-forward automatic gauge control in hot strip finishing mill. *Iron and Steel Institute of Japan (ISIJ) International*, 47(10):1444–1451, 2007.

[18] Y. K. Lee, S. W. Kim, and S. C. Hong. Modified feed-forward automatic gauge control using adaptive line enhancer in hot strip finishing rolling. In *Proceedings of the 29th Annual Conference of the IEEE Industrial Electronics Society (IECON '03)*, volume 3, pages 2233–2238, Roanoke, USA, 2003.

[19] A. Malik and J. Hinton. Displacement of multiple, coupled Timoshenko beams in discontinuous nonlinear elastic contact, with application to rolling mills. *Journal of Manufacturing Science and Engineering*, 134(5):051009 1–10, 2012.

[20] R. Nandan, R. Rai, R. Jayakanth, S. Moitra, N. Chakraborti, and A. Mukhopadhyay. Regulating crown and flatness during hot rolling: A multiobjective optimization study using genetic algorithms. *Materials and Manufacturing Processes*, 20(3):459–478, 2005.

[21] G. Pin, V. Francesconi, F. A. Cuzzola, and T. Parisini. Adaptive task-space metal strip-flatness control in cold multi-roll mill stands. *Journal of Process Control*, 23(2):108–119, 2013.

[22] K. Prinz, F. Schausberger, A. Steinboeck, and A. Kugi. Feedforward control of lateral asymmetries in heavy-plate hot rolling us-

Post-print version of the article: K. Prinz, A. Steinboeck, and A. Kugi, "Optimization-based feedforward control of the strip thickness profile in hot strip rolling", *Journal of Process Control*, vol. 64, pp. 100–111, 2018, ISSN: 0959-1524. DOI: 10.1016/j.jprocont.2018.02.001
The content of this post-print version is identical to the published paper but without the publisher's final layout or copy editing.

ing vision-based position estimation. In *Proceedings of the 20th IFAC World Congress*, volume 50, pages 11307–11312, Toulouse, France, 2017.

[23] K. Prinz, A. Steinboeck, M. Müller, A. Ettl, and A. Kugi. Automatic gauge control under laterally asymmetric rolling conditions combined with feedforward. *IEEE Transactions on Industry Applications*, 53(3):2560–2568, 2017.

[24] G. Rigler, H. Aberl, W. Staufer, K. Aistleitner, and K. Weinberger. Improved rolling mill automation by means of advanced control techniques and dynamic simulation. *IEEE Transactions on Industry Applications*, 32(3):599–607, 1996.

[25] D. Rosenthal. CVC technology on hot and cold strip rolling mills. *Revue de Métallurgie*, 85(7):597–606, 1988.

[26] F. Schausberger, A. Steinboeck, and A. Kugi. Optimization-based reduction of contour errors of heavy plates in rolling. *Journal of Process Control*, 47:150–160, 2016.

[27] R. Sims. The calculation of roll force and torque in hot rolling mills. *Proceedings of the Institute of Mechanical Engineers*, 168:191–200 and 209–214, 1954.

[28] A. Steinboeck, A. Kugi, and H. Mang. Energy-consistent shear coefficients for beams with circular cross sections and radially inhomogenous materials. *International Journal of Solids and Structures*, 50(11-12):1859–1868, 2013.

[29] C. Sun, C. Yun, J. Chung, and S. Hwang. Investigation of thermomechanical behavior of a work roll and of roll life in hot strip rolling. *Metallurgical and Materials Transactions A: Physical Metallurgy and Materials Science*, 29(9):2407–2424, 1998.

[30] R. Takahashi. State of the art in hot rolling process control. *Control Engineering Practice*, 9(9):987–993, 2001.

Post-print version of the article: K. Prinz, A. Steinboeck, and A. Kugi, "Optimization-based feedforward control of the strip thickness profile in hot strip rolling", *Journal of Process Control*, vol. 64, pp. 100–111, 2018, ISSN: 0959-1524. DOI: 10.1016/j.jprocont.2018.02.001
The content of this post-print version is identical to the published paper but without the publisher's final layout or copy editing.

Research highlights.

- A mathematical model for a hot strip tandem mill is developed and validated.
- A new optimization-based feedforward thickness controller is developed.
- A tailored numerically efficient solution of the optimization problem is presented.
- Simulation scenarios demonstrate the performance improvement of the proposed control concept.
- Promising results are obtained from a first installation of the control concept in the industrial plant.

Graphical abstract.

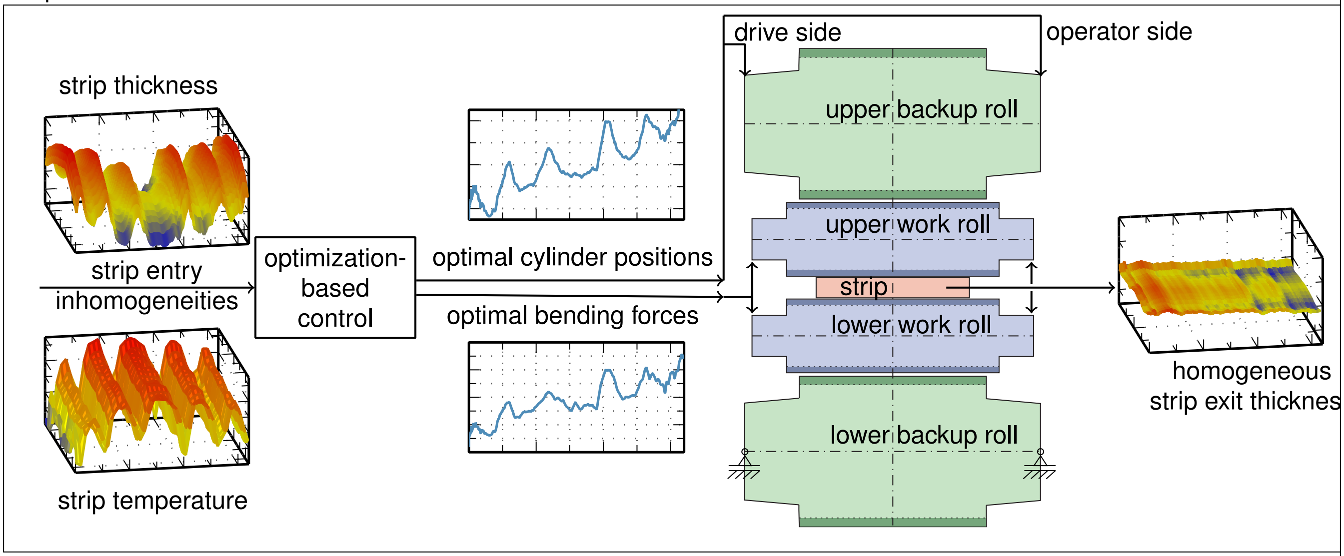

Post-print version of the article: K. Prinz, A. Steinboeck, and A. Kugi, "Optimization-based feedforward control of the strip thickness profile in hot strip rolling", *Journal of Process Control*, vol. 64, pp. 100–111, 2018, ISSN: 0959-1524. DOI: 10.1016/j.jprocont.2018.02.001
The content of this post-print version is identical to the published paper but without the publisher's final layout or copy editing.